Supporting Information

Zinc-doped C_4N_3/BiOBr S-scheme heterostructured hollow spheres for efficient photocatalytic degradation of tetracycline

Yaqi Liu[1, 2], Guicheng Luo[2, 3], Yichen Liu [1, 2], Zuozheng Xu [1, 2],

Hengxin Shen[2], Yuxiang Sheng[2], Yuan Zhu[2], Shuyi Wu[4, *], Lizhe Liu[1, *], Yun Shan[2, *]

[1]*Key Laboratory of Modern Acoustics, MOE, Institute of Acoustics and Collaborative Innovation Center of Advanced Microstructures, National Laboratory of Solid State Microstructures, Nanjing University, Nanjing, 210093, China*

[2]*Nanjing Key Laboratory of Advanced Functional Materials, Nanjing Xiaozhuang University, Nanjing 211171, People's Republic of China*

[3]*School of Chemistry and Chemical Engineering, Nantong University, Nantong 226019, China*

[4]*Jiangsu Key Laboratory of Micro and Nano Heat Fluid Flow Technology and Energy Application, School of Physical Science and Technology, Suzhou University of Science and Technology, Suzhou, 215009, People's Republic China*

[*]E-mail: wsy@usts.edu.cn (S.Y. Wu), lzliu@nju.edu.cn (L.Z. Liu)
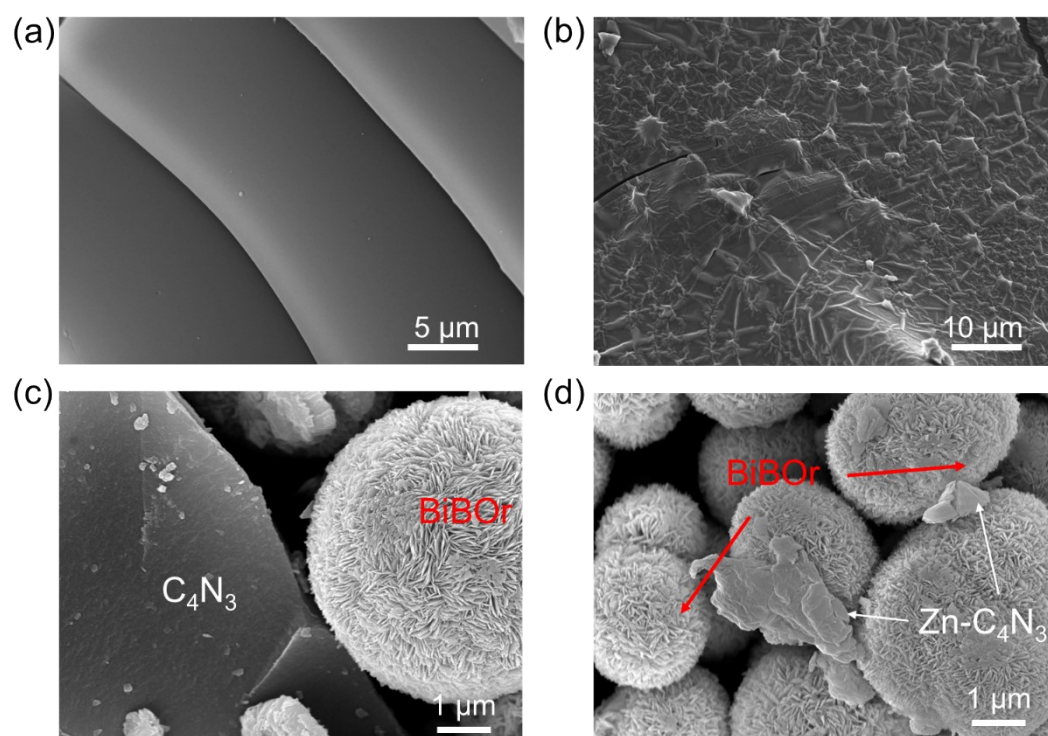or yshan@njxzc.edu.cn (Y. Shan)

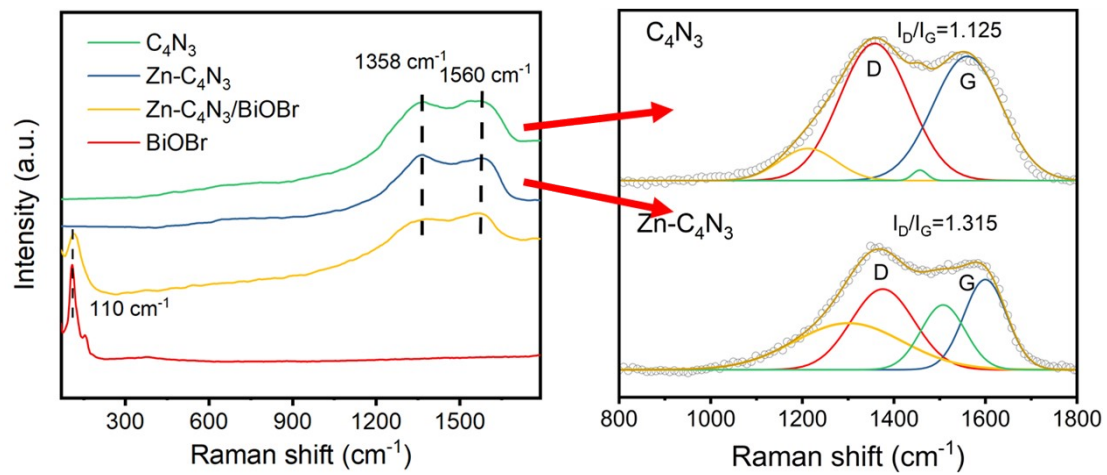**Fig. S1.** SEM images of (a) C_4N_3, (b) Zn-C_4N_3, (c) C_4N_3/BiOBr, (d) Zn-C_4N_3/BiOBr

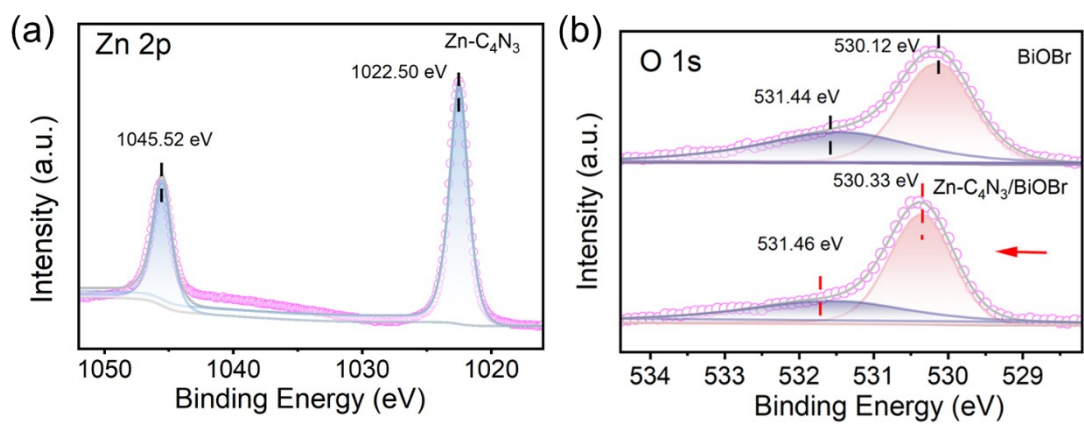**Fig. S2.** Raman spectra of C_4N_3, Zn-C_4N_3, C_4N_3/BiOBr and Zn-C_4N_3/BiOBr.

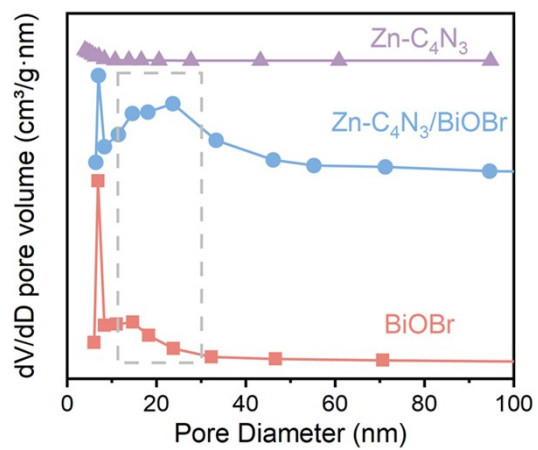**Fig. S3.** (a) The Zn 2p XPS spectra of Zn-C$_4$N$_3$. (b) The O 1s XPS spectra of BiOBr and Zn-C$_4$N$_3$/BiOBr.

Fig. S4. Pore size distribution curves of BiOBr, Zn-C$_4$N$_3$ and Zn-C$_4$N$_3$/BiOBr.
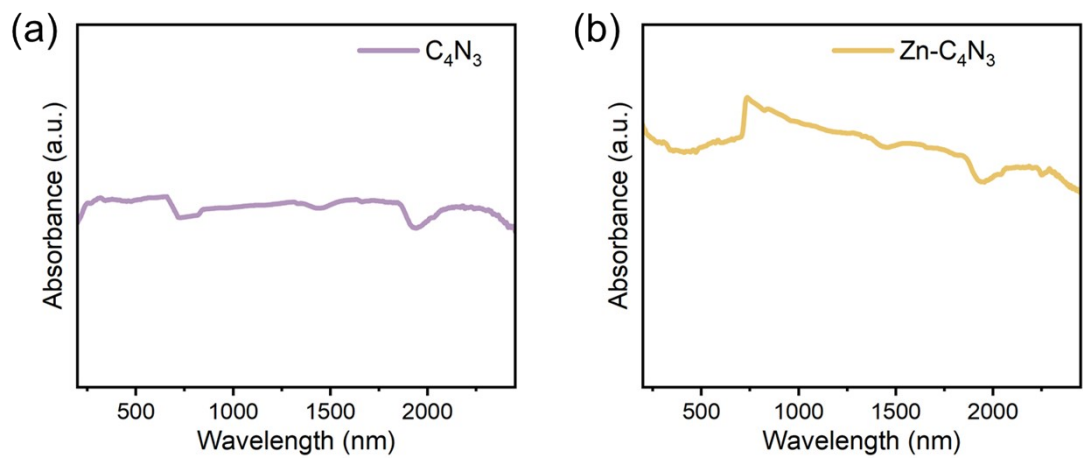
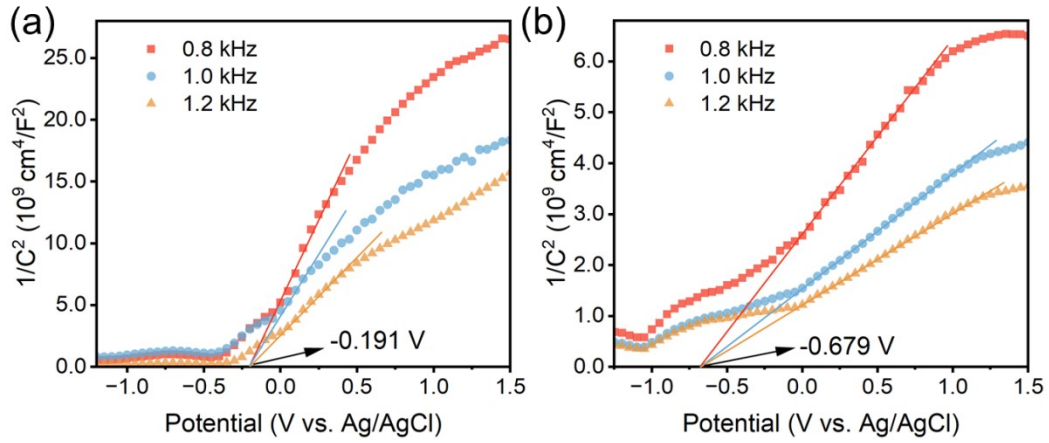**Fig. S5.** UV-vis absorption spectra of C_4N_3, Zn-C_4N_3 in the range of 200-2500nm.

Fig. S6. Mott-Schottky curves of (a) BiOBr and (b) Zn-C_4N_3.

The flat band potential E_{FB} is determined by employing Mott-Schottky plots, which involves measuring the capacitance at frequencies of 800Hz, 1000Hz and 1200Hz under dark conditions at the solid-liquid interface. This determination is based on the relation between the inverse of the square of the capacitance and the potential, as described by the following equation [1]:

$$1/C^2 = 2(E_a - E_{FB} - \kappa T/e) / (eN\varepsilon_0\varepsilon_s A^2)$$

where C is the capacity pertaining to space charge, E_a is the applied potential, E_{FB} is the flat band potential that can be ascertained through the process of extrapolation to a capacitance of zero, κ is the Boltzmann constant, T is the absolute temperature, e is the electron charge, N is the density of carriers, ε_0 is the electric permittivity of free space, ε_s is the dielectric constant of materials, and A is the area of electrode.
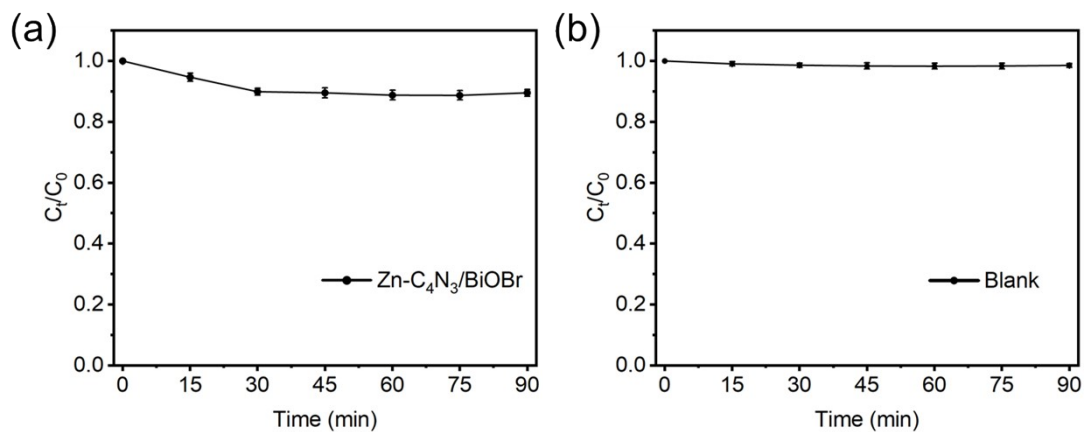
Fig. S7. (a) Degradation curve of TC under visible light irradiation for 90 min without the introduction of catalyst (TC: 25 mg/L). (b) Degradation curve of TC in the absence of light within 90 min (TC: 25 mg/L, Zn-C$_4$N$_3$/BiOBr: 20 mg).
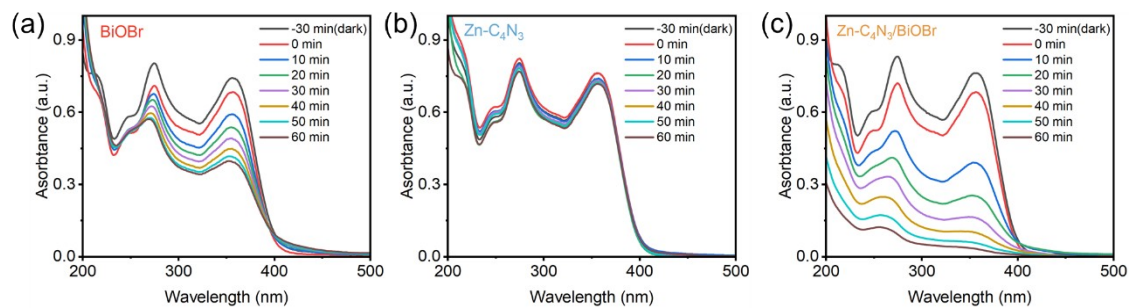
Fig. S8. The UV-Vis absorption spectra of degradation over (a) BiOBr (b) Zn-C$_4$N$_3$ (c) Zn-C$_4$N$_3$/BiOBr.
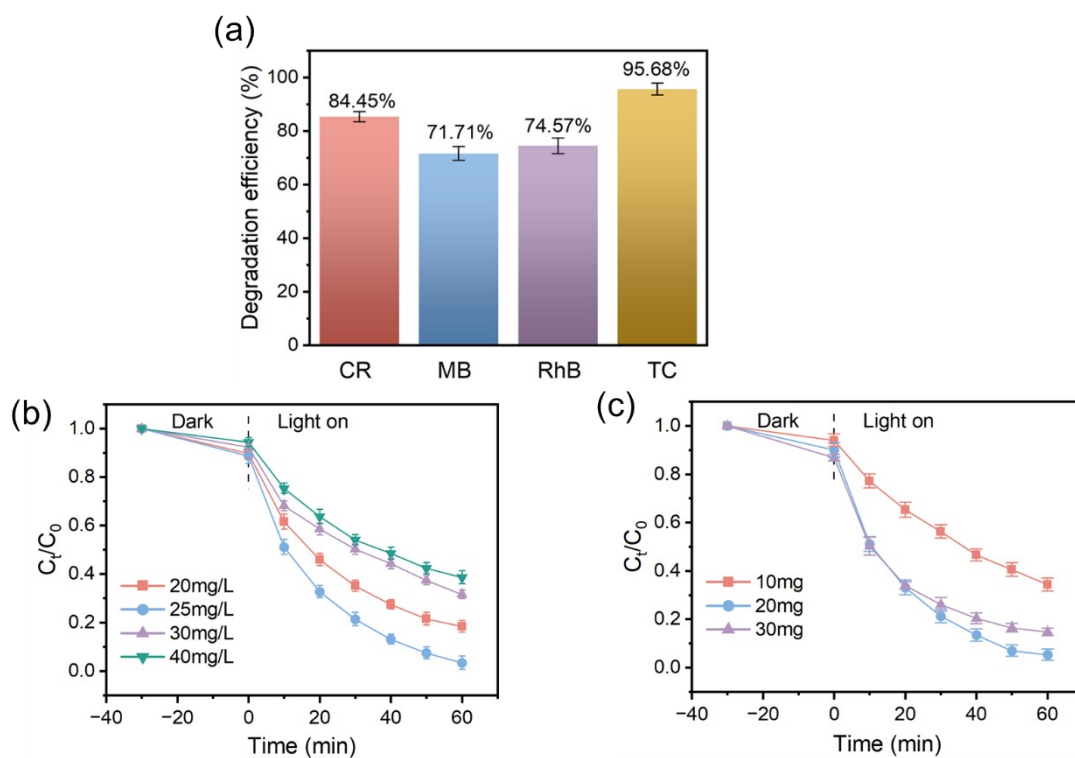
Fig. S9. (a) Photocatalytic degradation efficiency of different contaminants (CR, MB, RhB and TC by Zn-C$_4$N$_3$/BiOBr. Effect of (b) initial TC concentration and (c) catalyst dosage over Zn-C$_4$N$_3$/BiOBr in degradation of TC.

Fig. S10. (a) The SEM image and (b) XRD pattern of Zn-C$_4$N$_3$/BiOBr after cycling five times photocatalytic process.

Fig. S11. ESR spectra of DMPO - •OH deionized water solution over Zn-C$_4$N$_3$/BiOBr after irradiation.

Fig. S12. Mass spectra of TC and intermediates obtained after degradation at 10min and 50min under visible light irradiation.

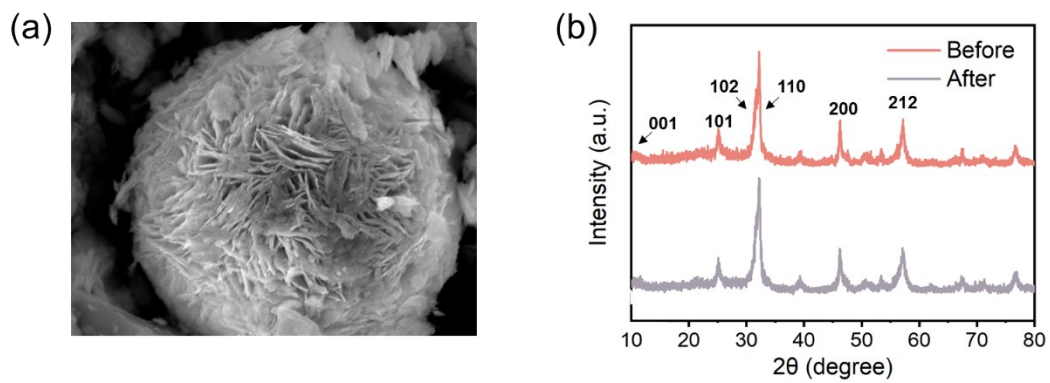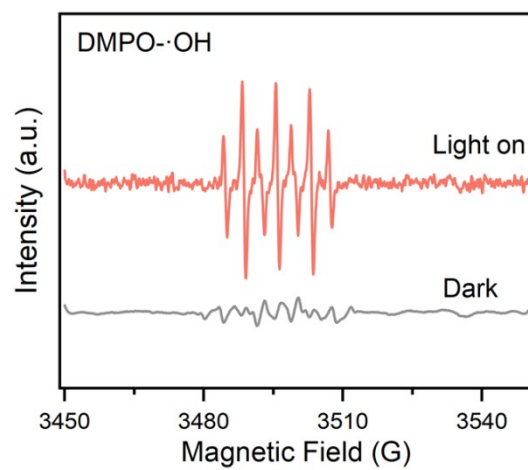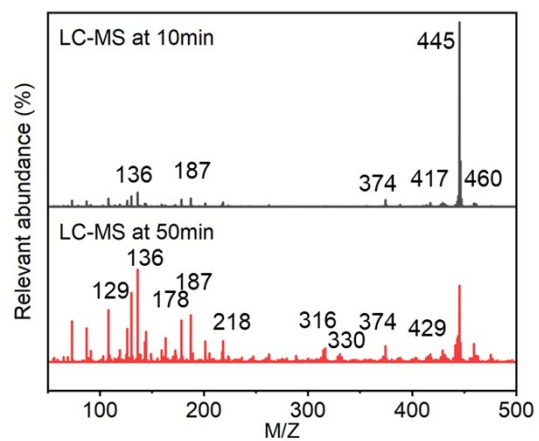The curves of time-resolved PL spectra are fitted by a biexponential function. The fitting equation is as follows [2]:

$$\Delta R/R_0(t) = A_1 \exp(-t/\tau_1) + A_2 \exp(-t/\tau_2)$$

where parameters τ_1 and τ_2 are the carrier lifetimes, and A1 and A2 are the corresponding proportion.

The fitting of photoluminescence decay profiles was conducted. A double exponential model was employed to fit the decay profiles of the prepared samples. The equation used to calculate the verage lifetime of photogenerated carriers is as follows：

$$\tau_{av} = (A_1 \cdot t_1^2 + A_2 \cdot t_2^2) / (A_1 \cdot t_1 + A_2 \cdot t_2)$$

where parameters τ_{av}, τ_1 and τ_2 are the carrier lifetimes, and A1 and A2 are the corresponding proportion.

Table S1. Parameters and the calculated decay times of A, t and τ via bi-exponential decay fitting for Zn-C$_4$N$_3$, BiOBr and Zn-C$_4$N$_3$/BiOBr.

Sample	τ_1 (ns)	A_1	τ_2 (ns)	A_2	τ_{av} (ns)	K (ns^{-1})
BiOBr	1.38	456.8	12.06	65.0	7.30	0.137
Zn-C$_4$N$_3$/BiOBr	0.62	383.3	4.43	131.2	3.33	0.300
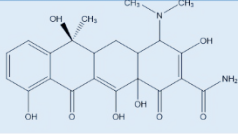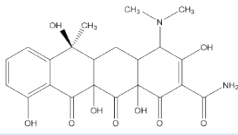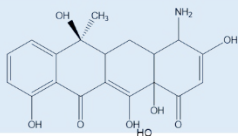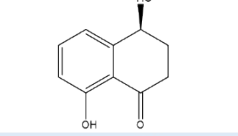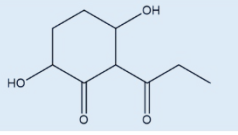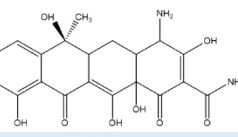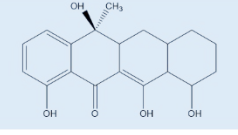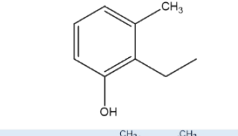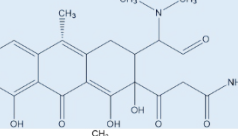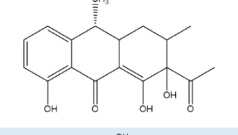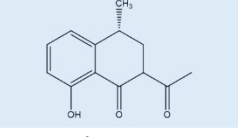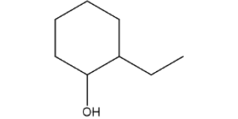
Table S2. The reaction rate and degradation efficiency of TC degradation by different catalysts.

Catalyst	TC concentration	Reaction time	Reation rate	Degradation efficiency	Refs.
Zn-C$_4$N$_3$/BiOBr	25 mg/L	60 min	4.96×10^{-2} min^{-1}	95.70%	This work
BT/BiOBr/Bi	20 mg/L	120 min	1.5×10^{-2} min^{-1}	93%	3
ZnO/BiOBr	20 mg/L	90 min	1.03×10^{-2} min^{-1}	86.76%	4
5NCDs/BiOBr	20 mg/L	60 min	4.2×10^{-2} min^{-1}	92%	5
BiOBr/Bi$_2$WO$_6$-0.2	20 mg/L	60 min	3.49×10^{-2} min^{-1}	88.06%	6
BiVO$_4$/BiOBr	10 mg/L	140 min	1.59×10^{-2} min^{-1}	90.4%	7
12%Zn-BiOBr	50 mg/L	180 min	0.28×10^{-2} min^{-1}	50.36%	8
NiTiO$_3$-BiOBr	40 mg/L	180 min	/	73.5%	9
20% Ni doped SnS$_2$/BiOBr	15 mg/L	70 min	4.88×10^{-2} min^{-1}	96.18%	10
Ag$_3$PO$_4$@MWCNTs@PPy	20 mg/L	6 min	1.67 min^{-1}	100%	11
Fe-N/C+PMS	11.1 mg/L	30 min	2.12×10^{-1} min^{-1}	100%	12

Table S3. Fukui index of TC.

Atom	q(N)	q(N+1)	q(N-1)	f⁻	f⁺	f⁰
1 (C)	-0.0721	-0.1011	-0.0428	0.0293	0.0290	0.0291
2 (C)	-0.0287	-0.0832	0.0035	0.0322	0.0545	0.0434
3 (C)	-0.0568	-0.0796	-0.0145	0.0424	0.0228	0.0326
4 (C)	0.0097	-0.0157	0.0180	0.0083	0.0254	0.0169
5 (C)	-0.0327	-0.0456	-0.0115	0.0212	0.0129	0.0170
6 (C)	0.0909	0.0658	0.1220	0.0311	0.0251	0.0281
7 (C)	0.0883	0.0866	0.0893	0.0010	0.0016	0.0013
8 (C)	-0.0267	-0.0292	-0.0213	0.0054	0.0025	0.0039
9 (C)	-0.0648	-0.0804	-0.0207	0.0442	0.0155	0.0299
10 (C)	0.1303	0.0638	0.1392	0.0089	0.0665	0.0377
11 (C)	-0.0567	-0.0618	-0.0510	0.0057	0.0051	0.0054
12 (C)	-0.0193	-0.0207	-0.0169	0.0023	0.0014	0.0019
13 (C)	0.0698	0.0624	0.0765	0.0066	0.0074	0.0070
14 (C)	0.1029	0.0572	0.1253	0.0224	0.0457	0.0340
15 (C)	0.0264	0.0205	0.0347	0.0084	0.0059	0.0071
16 (C)	0.1085	0.0631	0.1162	0.0077	0.0454	0.0266
17 (C)	-0.0797	-0.0972	-0.0640	0.0157	0.0175	0.0166
18 (C)	0.1351	0.1114	0.1471	0.0120	0.0236	0.0178
19 (O)	-0.1713	-0.1896	-0.1247	0.0466	0.0183	0.0325
20 (O)	-0.2350	-0.3077	-0.2094	0.0256	0.0727	0.0491
21 (O)	-0.1723	-0.2132	-0.1281	0.0442	0.0409	0.0425
22 (O)	-0.2422	-0.2824	-0.1968	0.0454	0.0402	0.0428
23 (O)	-0.2190	-0.2406	-0.2038	0.0152	0.0215	0.0184
24 (C)	0.1736	0.1558	0.1819	0.0082	0.0179	0.0131
25 (N)	-0.1445	-0.1585	-0.1328	0.0118	0.0140	0.0129
26 (O)	-0.2654	-0.2993	-0.2352	0.0302	0.0340	0.0321
27 (O)	-0.1618	-0.1957	-0.1498	0.0120	0.0339	0.0230
28 (N)	-0.0908	-0.0939	-0.0127	0.0781	0.0031	0.0406
29 (C)	-0.0446	-0.0482	-0.0279	0.0167	0.0037	0.0102
30 (C)	-0.0418	-0.0473	-0.0231	0.0187	0.0054	0.0121
31 (O)	-0.2194	-0.2311	-0.2092	0.0102	0.0117	0.0110
32 (C)	-0.0935	-0.0994	-0.0889	0.0046	0.0059	0.0052
33 (H)	0.0417	0.0200	0.0616	0.0199	0.0217	0.0208
34 (H)	0.0489	0.0212	0.0698	0.0208	0.0277	0.0243
35 (H)	0.0407	0.0234	0.0590	0.0183	0.0172	0.0178
36 (H)	0.0281	0.0189	0.0409	0.0128	0.0092	0.0110
37 (H)	0.0279	0.0214	0.0366	0.0087	0.0064	0.0076
38 (H)	0.0258	0.0134	0.0340	0.0081	0.0125	0.0103
39 (H)	0.0316	0.0267	0.0359	0.0043	0.0049	0.0046
40 (H)	0.0455	0.0327	0.0557	0.0102	0.0127	0.0115
41 (H)	0.1815	0.1638	0.2023	0.0208	0.0177	0.0192
42 (H)	0.1378	0.1243	0.1495	0.0118	0.0135	0.0126
43 (H)	0.1677	0.1568	0.1779	0.0102	0.0109	0.0105
44 (H)	0.1323	0.1159	0.1466	0.0143	0.0164	0.0154
45 (H)	0.1292	0.1202	0.1350	0.0058	0.0090	0.0074
46 (H)	0.1386	0.1268	0.1480	0.0094	0.0118	0.0106
47 (H)	0.0330	0.0329	0.0441	0.0111	0.0002	0.0056
48 (H)	0.0354	0.0237	0.0548	0.0194	0.0117	0.0155
49 (H)	0.0136	0.0073	0.0417	0.0281	0.0064	0.0172
50 (H)	0.0354	0.0302	0.0508	0.0154	0.0052	0.0103
51 (H)	0.0315	0.0202	0.0518	0.0203	0.0113	0.0158
52 (H)	0.0185	0.0108	0.0476	0.0291	0.0077	0.0184
53 (H)	0.1589	0.1484	0.1663	0.0074	0.0105	0.0089
54 (H)	0.0354	0.0340	0.0383	0.0028	0.0014	0.0021
55 (H)	0.0349	0.0231	0.0456	0.0107	0.0117	0.0112
56 (H)	0.0298	0.0186	0.0377	0.0078	0.0113	0.0095

Table S4. Intermediates of TC identified by LC-MS within 10 min and 50 min.

Structure NO.	Molecular Formula	M/Z	Probable Structure
TC	$C_{22}H_{24}N_2O_8$	445	
P1	$C_{22}H_{24}N_2O_9$	460	
P2	$C_{19}H_{19}NO_7$	374	
P3	$C_{10}H_{10}O_3$	178	
P4	$C_9H_{14}O_4$	187	
P5	$C_{20}H_{20}N_2O_8$	417	
P6	$C_{19}H_{22}O_5$	330	
P7	$C_9H_{12}O$	136	
P8	$C_{22}H_{24}N_2O_7$	429	
P9	$C_{18}H_{20}O_5$	316	
P10	$C_{13}H_{14}O_3$	218	
P11	$C_8H_{16}O$	129	

References

(1) Men, X.; Shan, Y.; Xu, Z.; Liu, L.; Wu, X. Multi-electron-channel integration to accelerate photogenerated carrier reaction kinetics for efficient sulfadiazine degradation. *Applied Catalysis A: General.* **2022**, *633*, 118513. DOI: 10.1016/j.apcata.2022.118513.

(2) Wu, Q.; Ma, H.; Wang, Y.; Chen, J.; Dai, J.; Xu, X.; Wu, X. Surface Electron Localization in Cu-MOF-Bonded Double-Heterojunction Cu_2O Induces Highly Efficient Photocatalytic CO_2 Reduction. *ACS Appl Mater Interfaces.* **2022**, *14* (48), 54328-54337. DOI: 10.1021/acsami.2c15278.

(3) Sun, J.; He, M.; Zhang, J.; Fu, T.; Huang, G.; Wang, L.; Liu, K.; Tong, Z.; Zhang, H. Insight into the synergistic effect of metal surface plasmon resonance and clay loading to boost the antibiotics degradation of Bentonite/BiOBr/bismuth. *Materials Science in Semiconductor Processing.* **2023**, *166*, 107739. DOI: 10.1016/j.mssp.2023.107739.

(4) Zhang, S.; Zhao, M.; Xu, C.; Mo, S.; He, J.; Long, F. Core-shell ZnO/BiOBr p-n heterojunction with excellent photocatalytic performance in degradation of tetracycline hydrochloride. *Materials Research Bulletin.* **2024**, *170*, 112545. DOI: 10.1016/j.materresbull.2023.112545.

(5) Chen, J.; zhang, Y.; Li, X.; Wang, Y.; Ma, C.; Guo, M. Ultrathin NCDs/BiOBr with oxygen vacancies for efficient photocatalytic degradation of tetracyclines: Revealing the triple role of NCDs in the synthesis. *Colloids and Surfaces A: Physicochemical and Engineering Aspects.* **2023**, *676*, 132276. DOI: 10.1016/j.colsurfa.2023.132276.

(6) Tang, D.; Chen, X.; Yan, J.; Xiong, Z.; Lou, X.; Ye, C.; Chen, J.; Qiu, T. Facile one-pot synthesis of a $BiOBr/Bi_2WO_6$ heterojunction with enhanced visible-light photocatalytic activity for tetracycline degradation. *Chinese Journal of Chemical Engineering.* **2023**, *53*, 222-231. DOI: 10.1016/j.cjche.2022.02.018.

(7) Singla, S.; Devi, P.; Basu, S. Revolutionizing the Role of Solar Light Responsive $BiVO_4$/BiOBr Heterojunction Photocatalyst for the Photocatalytic Deterioration of Tetracycline and Photoelectrocatalytic Water Splitting. *Materials (Basel).* **2023**, *16*, 5661. DOI: 10.3390/ma16165661.

(8) Zhang, J.; Jin, Y.; Zhang, Y.; Zhang, J.; Liu, Z.; Cai, Y.; Zhang, S.; Fang, M.; Kong, M.; Tan, X. The effect of internal stress on the photocatalytic performance of the Zn doped BiOBr

photocatalyst for tetracycline degradation. *Journal of the Taiwan Institute of Chemical Engineers.* **2023**, *143,* 104710. DOI: 10.1016/j.jtice.2023.104710.

(9) Sun, K.; Li, M.; Zhou, H.; Ma, X.; Li, W. Porous Rod-like $NiTiO_3$-BiOBr Heterojunctions with Highly Improved Visible-Light Photocatalytic Performance. *Materials (Basel).* **2023**, *16*, 5033. DOI: 10.3390/ma16145033.

(10) Li, Q.; Wang, L.; Song, J.; Huang, Y.; Xie, G.; Liu, Y.; Li, H. Novel 2D/2D S-scheme Ni doped SnS_2/BiOBr heterostructures with enhanced photocatalytic activity. *Arabian Journal of Chemistry.* **2023**, *16*, 105081. DOI: 10.1016/j.arabjc.2023.105081.

(11) Lin, Y.; Wu, X.; Han, Y.; Yang, C.; Ma, Y.; Du, C.; Teng, Q.; Liu, H.; Zhong, Y. Spatial separation of photogenerated carriers and enhanced photocatalytic performance on Ag_3PO_4 catalysts via coupling with PPy and MWCNTs. *Applied Catalysis B: Environmental* **2019**, *258*. DOI: 10.1016/j.apcatb.2019.117969.

(12) Wu, S.; Yang, Z.; Zhou, Z.; Li, X.; Lin, Y.; Cheng, J. J.; Yang, C. Catalytic activity and reaction mechanisms of single-atom metals anchored on nitrogen-doped carbons for peroxymonosulfate activation. *J Hazard Mater* **2023**, *459*, 132133. DOI: 10.1016/j.jhazmat.2023.132133.